Nanoscale

Accepted Manuscript

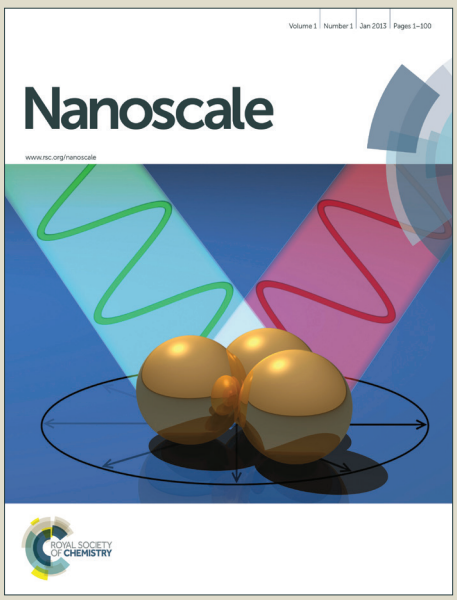

ROYAL SOCIETY OF CHEMISTRY

www.rsc.org/nanoscale

Journal Name

RSCPublishing

COMMUNICATION

Sub-bandgap transverse frequency conversion in semiconductor nano-waveguides

Cite this: DOI: 10.1039/x0xx00000x

Fuxing Gu,[a] Li Zhang,[a] Guoqing Wu,[a] Yingbin Zhu,[b] and Heping Zeng*[ac]

Received 00th January 2012,
Accepted 00th January 2012

DOI: 10.1039/x0xx00000x

www.rsc.org/

Abstract

Transverse frequency conversion in the sub-bandgap spectral region is investigated in semiconductor nanowires and nanoribbons by using CW lasers with pump power less than 1 mW. It is found that the properties of the emissions are strongly dependent on the cross-sectional geometries and the surrounding media of nano-waveguides. The polarization is higher in nano-waveguides under single-mode condition; and the spatial distribution is more tunable in nano-waveguides with higher-order modes involved. Compared with birefringent approach, transverse frequency conversion shows lower divergence angles, higher polarization, and more tunable spatial distribution.

Keywords: Transverse frequency conversion, Sub-bandgap, Nano-waveguides, Semiconductor

1. Introduction

Nano-waveguides (N-WGs) fabricated from a variety of materials such as glasses, inorganic crystals and semiconductors, are emerging as promising building blocks for nonlinear optical applications due to their tight confinement and tailorable waveguide dispersion.[1–5] Of the well-studied N-WGs, chemically synthesized (e.g., vapour-liquid-solid growth[5,6]) free-standing semiconductor N-WGs are attractive due to their favourable properties including large nonlinear susceptibilities for low threshold pumping, large refractive indices for tight confinement of guided light, and material diversity for various spectral ranges. Over the past few years nonlinear optical frequency generation in semiconductor N-WGs has been reported including second-harmonic generation (SHG) and sum-frequency generation (SFG), most of which are based on birefringent phase matching and the generated waves are guided along the length directions of N-WGs.[7–9]

Due to the large refractive indices of semiconductor N-WGs, the endface reflectivity is usually large (e.g., over 0.1[10]) and will offer a backward reflected waves. The overlap of forward- and backward waves will induce transverse frequency conversion vertically to the waveguide surface (also be called as surface-emitting frequency conversion),[11–13] which shows great advantages such as high conversion efficiency and low pump power compared with those in birefringent technique.[14–16] When light is guided along the N-WGs, the cross-sectional geometries and the surrounding media of N-WGs have a great influence on propagation parameters such as propagation constant, effective index, and polarization,[17–19] which may induce different nonlinear optical phenomena from those in birefringent SHG. For example, supercontinuum has been recently realized in CdS nanoribbons but is difficult to be realized in CdS nanowires.[5] Therefore study of the influence of cross-sectional geometries and substrate effects on transverse frequency conversion in semiconductor N-WGs is important for understanding the light-matter interaction as well as device applications. Nevertheless, such investigation of geometrical nonlinear effect has not yet been reported. In addition, previous studies mostly focused on the above-bandgap spectral region of semiconductors, which experience large multiphoton-absorption induced photoluminescence and suffer from large absorption of generated light[12–15]. In this communication transverse frequency conversion in the sub-bandgap spectral region are studied in semiconductor nanowires and nanoribbons. Continuous-wave (CW) pump lasers are efficiently launched into the N-WGs using silica fiber tapers. The properties of the transverse SHG and SFG emissions including emitting direction, spatial distribution, and polarization are experimentally and theoretically investigated.

2. Experimental

Single-crystalline semiconductor nanowires and nanoribbons including CdS, ZnSe, and ZnO are synthesized using a chemical vapor deposition process.[5,6] Typical nanowires have hexagonal cross-sectional geometries (Fig. 1(a)) and typical nanoribbons have rectangular cross-sectional geometries (Fig. 1(c)). Figs. 1(b) and (d) show two transmission electron microscope (TEM) images of a CdS nanowire and a CdS nanoribbon respectively, in which uniform and smooth sidewalls are observed.

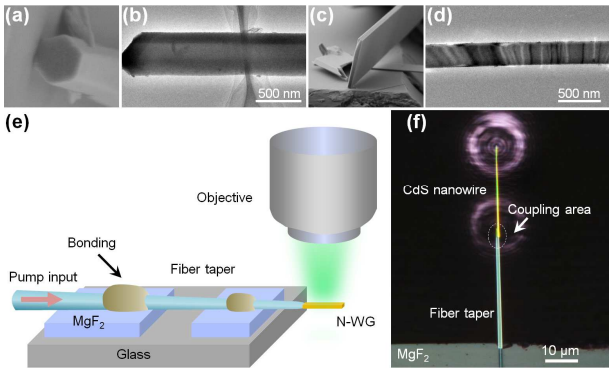

Fig. 1. Close-up SEM images of cross-sections, TEM images of as-grown CdS nanowires (a and b) and CdS nanoribbons (c and d), respectively. (e) Schematic diagram of an experimental setup for suspension coupling approach. (f) Optical micrograph of coupling a 1064-nm laser from a suspended silica fiber taper into a CdS nanowire.

As-grown N-WGs are placed on the tips of suspended silica optical fiber tapers via micromanipulation and pump light is coupled into the N-WGs based on an evanescent wave coupling technique.[19–21] For reference, this suspension coupling approach is schematically shown in Fig. 1(e), in which a fiber taper is placed in parallel and contact with one end of a N-WG (see experimental details in ref. 21). Fig. 1(f) provides an image of coupling a 1064-nm laser from a suspended silica fiber taper into a CdS nanowire. The bright light spot at the nanowire end indicates that pump light is efficiently coupled into the nanowire. To investigate the substrate effect,[19] N-WGs are also dispersed onto a MgF_2 substrate and silica optical fiber tapers are used to couple light into the N-WGs based on a butt coupling technique[5]. The pump sources used are CW monochromatic lasers. The generated emissions are collected using long working distance microscope objectives and directed to a spectrometer (QE65 Pro, Ocean Optics) and a CCD camera (DS-Ri1, Nikon). A short-pass emission filter (FF01-750/SP-25, Semrock) and a polarizer are used when taking CCD images and spectra.

3. Results and Discussion

Due to the high refractive indices of semiconductor N-WGs, some portion of the guided light is reflected by the endfaces and propagates backward. Then the forward ($_{+}\omega$) and backward ($_{-}\omega$) waves overlap and generate second-harmonic (SH) emission (2ω) on both lateral sides of N-WGs. Fig. 2(a) shows a schematic diagram of transverse SHG in a nanoribbon. Compared with birefringent SHG process that both SH waves

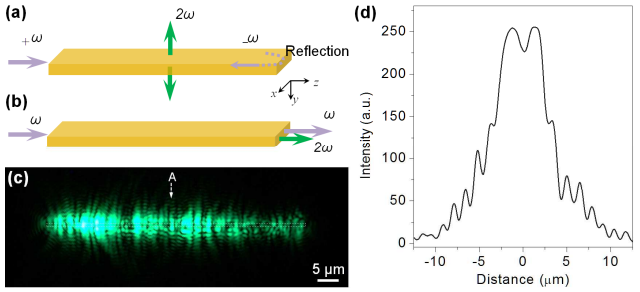

Fig. 2. Schematic diagrams of (a) transverse SHG and (b) birefringent SHG in a nanoribbon. (c) Optical micrograph of a SH emission from the lateral side of a 350-nm-thick ZnSe nanoribbon. (d) Spatially distributed intensity of the *A* pattern along the normal direction of the nanoribbon surface.

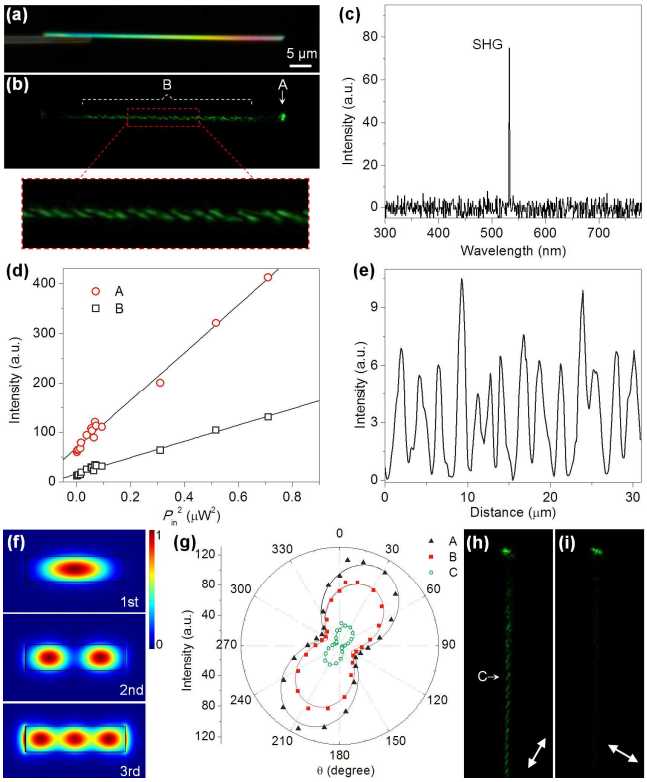

Fig. 3. Optical micrographs of a 1.24-μm-wide and 280-nm-thick CdS nanoribbon, which is supported by a suspended fiber taper and pumped by a 1064-nm laser. (c) Spectrum of *A* and *B* emissions. (d) Dependence of the I^{SH} as a function of P_{in}^2. (e) Spatial distribution of I^{SH} of *B* emission along the nanoribbon length direction. (f) Power distributions (Poynting vectors) of guided 1−3 order modes at the transverse cross plane of the CdSe nanoribbon. (g) φ-dependent I^{SH} of the *A* and *B* emissions. (h and i) Optical micrographs of the nanoribbon taken with $\varphi = 30°$ and 120°, respectively.

and fundamental waves are along the N-WG length direction (Fig. 2(b)), SH waves in the transverse SHG process are vertical to fundamental waves.[11–16] In this process, wavevectors of fundamental waves are automatically conserved in the plane of the N-WG surface. In the direction normal to the surface are not conserved, and the mismatching is equal to the SH wavevector. Fig. 2(c) shows an optical micrograph of a SH emission from the lateral side of a 350-nm-thick ZnSe

nanoribbon, which is pumped by a 1064-nm laser. It is clear that SH patterns are vertical to the nanoribbon surface and show symmetric on both sides of the nanoribbon. Fig. 2(d) shows the spatially distributed intensity of a typical emitting pattern (denoted as *A*) along the normal direction of the nanoribbon surface, which exponentially decays with an oscillation, suggesting that transverse SH intensity do not grow with propagation distance.[12,13] The propagation length (1/*e* damping intensity of the SH emission) is ~2.2 μm. A roughly measured divergence angle of the *A* pattern is less than 9°, which is much smaller than those in birefringent SHG (~50°).[22]

Fig. 3(a) shows an optical micrograph of a 1.24-μm-wide and 280-nm-thick CdS nanoribbon, which is suspended by a fiber taper and pumped by a 1064-nm laser with input power (P_{in}) of 300 μW. A bright green spot at the end of the nanoribbon (birefringent SHG, denoted as *A* in Fig. 3(b)) and periodical green patterns along the body (transverse SHG, denoted as *B*) are observed. Each pattern has an angle of ~30° with the nanoribbon axis (see enlarged image below). Fig. 3(c) shows that only 532 nm wavelength is detected, and Fig. 3(d) shows that the measured SH intensity (I^{SH}) of both of the *A* and the *B* emissions increase linearly with the square of the pump power (P_{in}^2), corresponding to their SHG nature. The spatial distribution of I^{SH} of the *B* emission along the nanoribbon length direction (Fig. 3(e)) exhibits an oscillation behavior with a period of ~2.2 μm and obeys the relationship of $I^{SH} \propto \cos^2(\Delta\beta z)$,[13] where β denotes the propagation constants and z denotes the position along the nanoribbon length direction. Calculation using Lumerical FDTD solution in Fig. 3(f) shows that the *B* emission arises from the counter-propagating waves of the second (β_2 = 10.9 μm^{-1}) and third order (β_3 = 9.4 μm^{-1}) guided modes which give a period of $\Lambda \approx \pi/\Delta\beta$ = 2.1 μm and agree well with the experimental result. The angle of ~30° between the patterns and the nanoribbon axis shown in Fig. 3(b) is also attributed to the overlap of different orders of guided modes. From many experimental results, it is found that the angles and the oscillation periods of patterns highly depend on the widths of the nanoribbons and the orders of the guided modes, as well as the refractive indices of surrounding media.

The polarization angle (φ) is defined as the cross angle changes between the length direction and the polarizer direction. Fig. 3(g) gives φ-dependent I^{SH} of the *A* and the *B* emissions, both of which exhibit similar oscillation behaviors between the maximum at φ = 30° and the almost zero at φ = 120°. Fig. 3(h) and 3(i) provide images of the nanoribbon taken at φ = 30° and 120°, respectively. The green circles plotted in Fig. 3(g) give φ-dependent I^{SH} of an individual pattern of the *B* emission (denoted as *C*), which has the same polarization direction as the *A* and the *B* emissions. The polarization ratio (ρ), defined as $\rho = (P_{max} - P_{min})/(P_{max} + P_{min})$,[19] of the *A* and *C* emissions are 0.61 and 0.83, respectively, suggesting that transverse SHG are more highly polarized than birefringent SHG.

Fig. 4(a) shows an optical micrograph of a 860-nm-diameter CdS nanowire, which is supported by a suspended fiber taper and pumped by a 1064-nm laser with P_{in} of 300 μW. Fig. 4(b) shows that a weak spot emits at the end of the nanowire (denoted as *A*) and a line emission emits along the nanowire length direction (denoted as *B*). Calculation shows that the *B* emission arises from two counter-propagating waves with the same order modes, and thus induces the line patterns with a very large period. Fig. 4(c) gives φ-dependent I^{SH} of the *A* and *B* emissions. It is noticed that the *B* emission exhibits an oscillation behavior between the maximum at φ = 0° and the minimum at φ = 90°, and *A* emission shows a different angle of ~21° in the polarization direction between *B* emission, which may induced by higher order modes guided in the nanowire. The ρ of the *A* and *B* emissions are 0.67 and 0.81, respectively, further suggesting the higher polarization of transverse SHG.

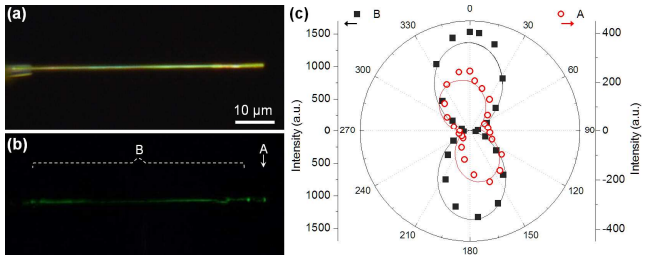

Fig. 4. Schematic (a and b) Optical micrographs of an 860-nm-diameter CdS nanowire, which is supported by a suspended fiber taper and pumped by a 1064-nm laser. (c) φ-dependent I^{SH} of the *A* and *B* emissions.

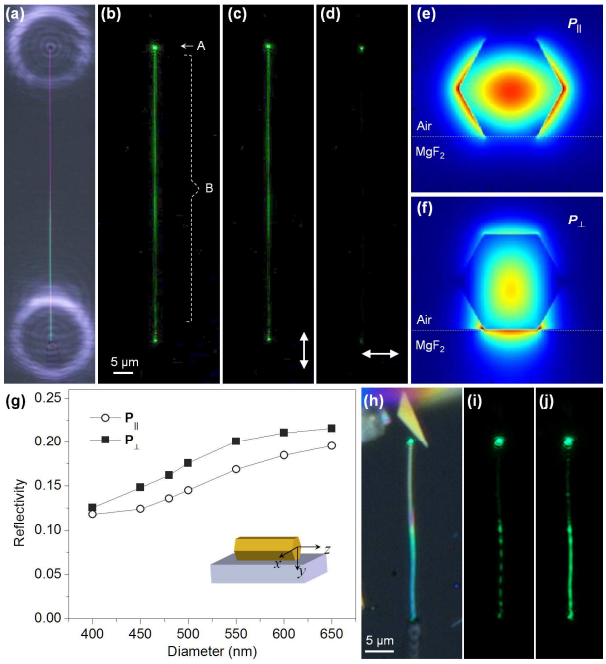

Fig. 5. (a and b) Optical micrographs of a 440-nm-diameter ZnO nanowire, which is supported by a MgF_2 substrate and pumped by a 1064-nm laser. (c and d) Optical micrographs of the nanowire taken with φ = 0° and 90°, respectively. (e and f) Power distributions (Poynting vectors) of guided $P_{\perp}$ and $P_{||}$ modes at the transverse cross plane of the ZnO nanowire. (g) Endface reflectivity of $P_{\perp}$ and $P_{||}$ modes in MgF_2 substrate-supported ZnO nanowires. (h, i, and j) Optical micrographs of SHG in a 670-nm-diameter ZnSe nanowire.

Figs. 5(a) and (b) show that in a 440-nm-diameter ZnO nanowire supported on a MgF_2 substrate and pumped by a 1064-nm laser, a bright spot emission at the upper end (denoted as *A*) and a line emission along the nanowire length (denoted as *B*) are observed. When $\varphi = 0°$ (Fig. 5(c)) the intensity of both of *A* and *B* emissions is maximum, and when $\varphi = 90°$ only the *A* light spot is observed (Fig. 5(d)). The ρ of the *A* emission is 0.36 and the ρ of the *B* emission is 0.92, which is higher than those in nanowires with larger diameters (Fig. 3) and nanoribbons with wider widths (Fig. 4). Calculation shows that in a 450-nm-diameter ZnO nanowire only lower-order mode can be efficiently guided, and the power of the guided lower-order mode with polarization vertical to substrate ($P_\perp$, Fig. 5(e)) suffers higher power leakage than that parallel to the substrate ($P_\parallel$, Fig. 5(f)).[19] In addition, calculation shows that the endface reflectivity of $P_\perp$ mode is lower than that of $P_\parallel$ mode (Fig. 5(g)) in ZnO nanowires at single mode condition.[17] Thus only $P_\parallel$ mode can be efficiently guided and reflected, and induces a line pattern along the nanowire length with much higher polarization of transverse SHG than those of higher-order modes involved transverse SHG and in birefringent SHG.

By using large diameter nanowires, the spatial distribution of transverse emissions along the nanowire can be tuned. Fig. 5(h) shows in a 670-nm-diameter ZnSe nanowire, $P_\perp$ mode can be efficiently guided and reflected, and overlaps with $P_\parallel$ mode, inducing patterns with a period of ~1.9 μm along the nanowire shown in Fig. 5(i). By varying the polarization of pump light, the period patterns are changed into a single line, as shown in Fig. 5(j). This effect is also observed in nanoribbons.

By coupling another pump laser from the other end of semiconductor N-WGs transverse SFG is also demonstrated. Figs. 6(a) and (b) show optical micrographs of a 690-nm-diameter ZnSe nanowire coupled with a 1064-nm laser from the left side and an 808-nm laser from the right side. A green line emission along the length and a bright green spot at the right end with a peak wavelength of 532 nm (Fig. 6(c)) are observed, corresponding to the transverse and birefringent SHG from the 1064-nm laser, respectively. Feather-like blue emissions with divergence angles less than 10° along the length and with a peak wavelength of 459 nm are also observed, corresponding to the transverse SFG signal of the 1064- and 808-nm lasers. Due to the difference of wavevectors of the two pump lasers, the direction of SFG is inclining to the surface normal of the nanowire, suggesting the potential application of wavelength discriminating by using the transverse SFG technique. From the φ-dependent intensity of SHG and SFG emissions shown in Fig. 6(d), there is a difference of ~10° in the maximum polarization direction between the 459-nm SFG and 532-nm SHG. The ρ of the SFG is 0.81 and the ρ of the SHG is 0.75.

4. Conclusion

In summary, sub-bandgap transverse SHG and SFG processes in semiconductor nanowires and nanoribbons are investigated by using CW lasers with pump power less than 1 mW. Compared with birefringent approach, transverse

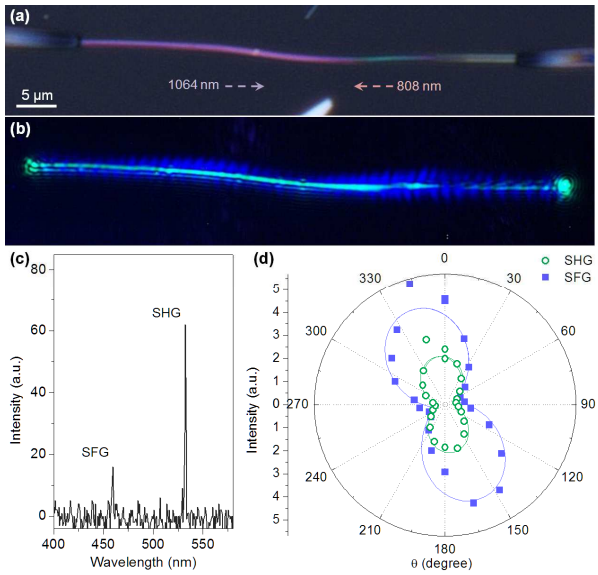

Fig. 6. (a and b) Optical micrographs of a MgF_2-supported 690-nm-diameter ZnSe nanowire coupled with a 1064-nm laser and an 808-nm laser. (c) Spectrum of generated emissions. (d) φ-dependent intensity of transverse 532-nm SHG and 459-nm SFG emissions.

frequency conversion shows attractive properties including lower divergence angles, higher polarization, and tunable spatial distribution, which are observed both in nanowire and nanoribbons. The polarization direction is higher in N-WGs under single-mode condition; and the spatial distribution is more tunable in N-WGs with higher-order modes involved. Due to the weak absorption of generated light, the sub-bandgap approach is more general and can be easily applied to other N-WGs such as inorganic crystals and metals,[23] which may achieve broadband and tunable compact nanoscale sources and spectroscopic studies.[24,25] Furthermore, the transverse frequency conversion takes places around the surface of N-WGs with wavelength-scale near-field interaction volume, which may facilitate attractive applications such as high spatial-resolution spectro-imaging and biomolecular sensing.

Acknowledgements

This work was partly supported by the National Natural Science Foundation of China (11304202 and 91221304), Natural Science Foundation of Shanghai (13ZR1458000), National Key Scientific Instrument Project (2012YQ150092), and National Basic Research Program of China (2011CB808105).

Notes and references

[a] Shanghai Key Laboratory of Modern Optical System, Engineering Research Center of Optical Instrument and System (Ministry of Education), School of Optical-Electrical and Computer Engineering, University of Shanghai for Science and Technology, Shanghai 200093, China. E-mail: hpzeng@phy.ecnu.edu.cn

[b] Engineering Product Development, Singapore University of Technology and Design Singapore, 138682, Singapore

[c] State Key Laboratory of Precision Spectroscopy, East China Normal University, Shanghai 200062, China

1 R. Yan, D. Gargas and P. Yang, *Nat. Photon*, 2009, **3**, 569.
2 M. A. Foster, A. C. Turner, M. Lipson and A. L. Gaeta, *Opt. Express*, 2008, **16**, 1300.
3 Y. Nakayama, P. J. Pauzauskie, A. Radenovic, R. M. Onorato, R. J. Saykally, J. Liphardt and P. Yang, *Nature*, 2007, **447**, 1098.
4 S. Leon-Saval, T. Birks, W. Wadsworth, P. St J Russell and M. Mason, *Opt. Express*, 2004, **12**, 2864.
5 F. Gu, H. Yu, W. Fang and L. Tong, *Opt. Express*, 2012, **20**, 8667.
6 F. Gu, Z. Yang, H. Yu, J. Xu, P. Wang, L. Tong and A. Pan, *J. Am. Chem. Soc.*, 2011, **133**, 2037.
7 C. Zhang, Z. Dong, G. You, R. Zhu, S. Qian, H. Deng, H. Cheng and J. Wang, *Appl. Phys. Lett.*, 2006, **89**, 042117-3.
8 T. Voss, J. P. Richters and A. Dev, *physica status solidi (b)*, 2010, **247**, 2476.
9 C. J. Barrelet, H.-S. Ee, S.-H. Kwon and H.-G. Park, *Nano Lett.*, 2011, **11**, 3022.
10 S. Wang, Z. Hu, H. Yu, W. Fang, M. Qiu and L. Tong, *Opt. Express*, 2009, **17**, 10881.
11 N. Bloembergen, H. Simon and C. Lee, *Phys. Rev.*, 1969, **181**, 1261.
12 Y. Beaulieu, S. Janz, H. Dai, E. Frlan, C. Fernando, A. Delâge, P. Van Der Meer, M. Dion and R. Normandin, *J. Nonlinear Opt. Phys.*, 1995, **4**, 893.
13 K. Shore, X. Chen and P. Blood, *Prog. Quant. Electron.*, 1996, **20**, 181.
14 R. Sanatinia, M. Swillo and S. Anand, *Nano Lett.*, 2012, **12**, 820.
15 W. Liu, K. Wang, Z. Liu, G. Shen and P. Lu, *Nano Lett.*, 2013, **13**, 4224.
16 H. Yu, W. Fang, X. Wu, X. Lin, L. Tong, W. Liu, A. Wang and Y. R. Shen, *Nano Lett.*, 2014, **14**, 3487.
17 L. Tong, J. Lou and E. Mazur, *Opt. Express*, 2004, **12**, 1025.
18 M. A. Foster, K. D. Moll and A. L. Gaeta, *Opt. Express*, 2004, **12**, 2880.
19 F. Gu, H. Yu, P. Wang, Z. Yang and L. Tong, *ACS Nano*, 2010, 4, 5332.
20 F. Gu, H. Zeng, L. Tong and S. Zhuang, *Opt. Lett.*, 2013, **38**, 1826.
21 F. Gu, H. Zeng, Y. Zhu, Q. Yang, L. Ang and S. Zhuang, *Adv. Optical Mater.*, 2013, **2**, 189.
22 F. Dutto, C. Raillon, K. Schenk and A. Radenovic, *Nano Lett.*, 2011, **11**, 2517.
23 Y. Shen, *IEEE J. Sel. Top. Quant.*, 2000, **6**, 1375.
24 J. Li, C. Meng, Y. Liu, X. Wu, Y. Lu, Y. Ye, L. Dai, L. Tong, X. Liu, and Q. Yang, *Adv. Mater.*, 2013, **25**, 833.
25 Z. Yang, D. Wang, C. Meng, Z. Wu, Y. Wang, Y. Ma, L. Dai, X. Liu, T. Hasan, X. Liu, and Q. Yang, *Nano Lett.*, 2014, **14**, 3153.